Partially ionized hydrogen plasma in strong magnetic fields

Alexander Y. Potekhin,[1,*] Gilles Chabrier,[2,†] and Yuri A. Shibanov[1]
[1]*Ioffe Physical-Technical Institute, 194021 St. Petersburg, Russia*
[2]*CRAL (UMR CNRS No. 5574), Ecole Normale Supérieure de Lyon, 69364 Lyon Cedex 07, France*
(Received 10 February 1999)

We study the thermodynamic properties of a partially ionized hydrogen plasma in strong magnetic fields, $B\sim10^{12}-10^{13}$ G, typical of neutron stars. The properties of the plasma depend significantly on the quantum-mechanical sizes and binding energies of the atoms, which are strongly modified by thermal motion across the field. We use new fitting formulas for the atomic binding energies and sizes, based on accurate numerical calculations and valid for any state of motion of the atom. In particular, we take into account decentered atomic states, neglected in previous studies of thermodynamics of magnetized plasmas. We also employ analytic fits for the thermodynamic functions of nonideal fully ionized electron-ion Coulomb plasmas. This enables us to construct an analytic model of the free energy. An ionization equilibrium equation is derived, taking into account the strong magnetic field effects and the nonideality effects. This equation is solved by an iteration technique. Ionization degrees, occupancies, and the equation of state are calculated. [S1063-651X(99)01308-2]

PACS number(s): 52.25.Kn, 05.70.Ce, 95.30.Qd, 97.60.Jd

I. INTRODUCTION

Magnetic fields $B\sim10^{12}-10^{13}$ G typical of isolated neutron stars qualitatively modify many physical properties of matter (see Refs. [1,2] for reviews). In this paper we calculate the thermodynamic properties of a strongly magnetized hydrogen plasma at temperature $T\sim10^{5.0}-10^{6.5}$ K, which may compose outer neutron-star envelopes [3–5]. As we shall see, the plasma under these conditions can be partially ionized, and the quantum-mechanical properties of both free electrons and bound species (primarily hydrogen atoms) are strongly modified by the field, which thereby affects the thermodynamics.

The motion of charged particles in a magnetic field is quantized into Landau orbitals. The magnetic field is called *strongly quantizing* if the free electrons populate mostly the ground Landau level [2]. This is the situation which we are especially interested in. It occurs when the electron cyclotron energy $\hbar\omega_c=\hbar eB/(m_ec)$ (where $\hbar$, e, m_e, and c are the Planck constant, electron charge, electron mass, and speed of light, respectively) exceeds both the thermal energy k_BT and the electron Fermi energy ϵ_F—that is, for temperatures $T\ll T_B$ and densities $\rho<\rho_B$, where

$$T_B=3.16\times10^5\gamma\ \text{K},\quad \rho_B=0.809\gamma^{3/2}\ \text{g cm}^{-3} \tag{1}$$

(see Sec. III A 1). Here, the parameter $\gamma=\hbar^3B/(m_e^2ce^3)=B/(2.35\times10^9\ \text{G})$ is the electron cyclotron energy in atomic units.

We will refer to a *strong* magnetic field when $\gamma\gg1$. A number of studies of the equation of state (EOS) of matter in strong magnetic fields were based on various modifications of the Thomas-Fermi approximation [6–9]. This approximation works reasonably well at large ρ and for large ion charge Z_i. Abrahams and Shapiro [8] estimate its validity range as $\rho\gg\rho_BZ_i^{-1/2}$. We consider $Z_i=1$ and lower densities, for which atoms are present in the plasma and contribute to the EOS.

The atom in a strong magnetic field $\gamma\gg1$ is compressed in the transverse directions to the size of the ''magnetic length'':

$$a_m=(\hbar c/eB)^{1/2}=a_0\gamma^{-1/2}, \tag{2}$$

where $a_0=\hbar^2/(m_ee^2)$ is the Bohr radius. The ground-state binding energy grows logarithmically with B and exceeds the ground-state energy of the field-free atom by order of magnitude at $B\sim10^{12}$ G [1]. Ionization equilibrium of atoms in strong magnetic fields was first discussed by Gnedin *et al.* [10] and Khersonskii [11]. Khersonskii [12] considered also dissociation equilibrium of H_2^+ species. However, these pioneering works neglected modifications of the atomic properties caused by the thermal motion of the atoms across the field.

The motional modifications of quantum-mechanical characteristics of the atom arise from the coupling between the center-of-mass motion across the field and the relative electron-proton motion [13–17]. The role of these effects was appreciated by Ventura *et al.* [18], who, however, did not treat them quantitatively. An increase of the nonionized fraction caused by the motion effects was mentioned by Pavlov and Mészáros [16], who used perturbation theory applicable to atoms only slightly distorted from their rest-state cylindrical shape. Quantum-mechanical calculations of binding energies and wave functions of hydrogen atoms in *any* states of motion in the strong magnetic fields have been carried out only recently [15,17].

Lai and Salpeter [19,20] evaluated the effects of motion on the ionization equilibrium using an approximation for the binding energies of moving atoms which does not apply to the so-called *decentered states*, for which the electron-proton separation is large [14,15,17]. Nonideality effects were included in the ionization equilibrium equation only as a pressure-ionization factor for $\rho\gg10^2$ g cm^{-3}. As a result,

*Eelectronic address: palex@astro.ioffe.rssi.ru
†Electronic address: chabrier@ens-lyon.fr

this equation contains a factor which diverges (and becomes even negative) at sufficiently high temperatures.

Recently, Steinberg *et al.* [21] calculated the second virial coefficient of the proton-electron plasma in arbitrary magnetic field and constructed an EOS at low densities. The bound states were included using the Planck-Larkin partition function. This approach yields correct EOS at the low density where the virial expansion holds [22]. However, the Planck-Larkin formalism fails at higher densities, where one has to resort to the chemical picture of the plasma, as discussed in detail, e.g., by Däppen *et al.* [23]. In addition, atomic binding energies were calculated in [21] using approximations [19] which have very restricted applicability as shown in [24].

In this paper we use new fitting formulas to atomic energies and sizes [24] based on a previous numerical study [17], valid for any state of atomic motion. The molecular H_2 fraction is evaluated following the approach of Lai and Salpeter [20] but with a modified treatment of nonideality. Our knowledge of the quantum-mechanical properties of molecules in a strong magnetic field is still incomplete, but an evaluation of the molecular fraction is useful to determine the validity domain of our EOS at relatively low temperatures (where the molecules dominate).

The next section presents a simple thermodynamic model of the hydrogen plasma. The model is tested in the nonmagnetic case by comparison with more elaborate models, and is shown to provide sufficient accuracy at high T where the molecular fraction is small. In Sec. III, we consider a fully ionized plasma in a strong magnetic field. The partial ionization and dissociation are discussed in Sec. IV, where an analytic model of the plasma free energy is constructed and the ionization equilibrium equation is derived. Numerical results are presented and discussed in Sec. V.

II. THERMODYNAMIC MODEL: THE ZERO-FIELD CASE

A. Chemical picture of the plasma

A theoretical description of partially ionized plasmas can be based either on the physical picture or on the chemical picture of the plasma [22]. In the chemical picture, bound species (atoms, etc.) are treated as elementary entities along with free electrons and nuclei. In the physical picture, nuclei and electrons (free and bound) are the only fundamental constituents of the thermodynamic ensemble. The relative merits of the two approaches have been discussed, e.g., in [25,26].

We use the so-called occupation probability formalism in frames of the chemical picture. Occupation probabilities, which ensure convergence of the internal partition functions (IPF), were first introduced by Fermi [27], who has demonstrated their immanent relation to a nonideal contribution in the Helmholtz free energy. Various approaches to the construction of the occupation probabilities have been reviewed by Hummer and Mihalas [28]. The approach adopted by Mihalas and co-workers [28–30] (hereafter MDH) is based on the Inglis-Teller criterion of Stark broadening conventional for plasma spectroscopy, which gives optical spectra consistent with available experiments (see, e.g., Ref. [23]). However, the equation of state derived by MDH is unrealistic at $\rho \gtrsim 10^{-2}\ \mathrm{g\,cm^{-3}}$ (see [31]), and the approximations made in its derivation are lacking in self-consistency [32]. An alternative EOS was derived in a self-consistent manner by Saumon and Chabrier [26,31,33,34] (hereafter SC) from effective pair potentials between plasma particles, but with neglect of the Stark broadening. The ionization degree deduced by SC strongly differs from that by MDH. The origin of the discrepancy is rooted in the fact that strongly perturbed atoms, whose spectral lines disappear due to the Stark merging, may still contribute to the EOS as bound species [35]. Thus the approaches of MDH and SC are reconciled by an approximate treatment of the atoms perturbed by plasma ions as quasicontinuum atomic states, which contribute to the EOS as atoms although they do not show atomic spectral lines [32].

The chemical picture faces a principal difficulty in cases where the interaction between nuclei and electrons in a bound state is comparable to the interaction between a bound object and neighboring plasma particles. This situation occurs when pressure ionization is important or when high atomic levels are appreciably populated. In these cases, a special term should be included into the free-energy model, in order to distinguish between bound and free states. For instance, MDH constructed an *ad hoc* ''pressure ionization term'' in the free energy [29], SC introduced hard cores with fixed diameters in the effective potentials for bound species [34], and exponential ''unbinding'' occupation probabilities were used in [32]. The latter approach has been justified by considering an excluded volume of the bound objects at relatively low density, assuming an uncorrelated distribution of the plasma particles. At high density, the strong correlations of the positions of the particles must be taken into account. Their approximate treatment in the hard-sphere model (e.g., by SC) appears to be practical for this purpose.

In the case of the strong magnetic field, the model of the plasma cannot be as detailed as, e.g., the SC nonmagnetic model, because the effective potentials (partly derived from high-pressure experiments in the zero-field case) are not available. Therefore we use a simple hard-sphere picture described below. In order to check the validity of this model, we apply the same assumptions to the well-studied zero-field case and compare the results with those of more elaborated models.

B. Free-energy model

Consider a plasma consisting of electrons, protons, and H atoms in a volume V. Let us write the Helmholtz free energy as $F = F_{\mathrm{id}} + F_{\mathrm{ex}}$, where

$$F_{\mathrm{id}} = F_{\mathrm{id}}^{(e)} + F_{\mathrm{id}}^{(p)} + F_{\mathrm{id}}^{\mathrm{neu}} + F_{\mathrm{rad}} \tag{3}$$

is the sum of the ideal-gas free energies of the electrons, protons, neutral species, and photons (thermal radiation), respectively, and F_{ex} is the *excess* (nonideal) part.

1. Ideal part of the free energy

We consider nondegenerate protons and neglect their spin statistics both in bound and free states (this amounts to an additive constant in the entropy that affects neither ionization equilibrium nor the EOS, provided the total number of free and bound protons, N_0, is fixed). Then

$$\beta F_{\mathrm{id}}^{(p)}/N_p = \ln(n_p \lambda_p^3) - 1, \tag{4}$$

where $\beta \equiv (k_B T)^{-1}$. Here and hereafter, N_α, n_α, and $\lambda_\alpha \equiv (2\pi\beta\hbar^2/m_\alpha)^{1/2}$ denote, respectively, the total number, number density, and thermal wavelength of particles of type α with mass m_α.

For the ideal gas of electrons, we use the identity [36]

$$F_{\rm id}^{(e)} = \mu_e N_e - P_e V, \tag{5}$$

where μ_e and P_e are the chemical potential and pressure of the ideal Fermi gas, respectively, which can be obtained as functions of n_e and T from the equations

$$P_e = \frac{8}{3\sqrt{\pi}} \frac{k_B T}{\lambda_e^3} I_{3/2}(\beta\mu_e), \tag{6}$$

$$n_e = \frac{4}{\sqrt{\pi}\lambda_e^3} I_{1/2}(\beta\mu_e). \tag{7}$$

Here,

$$I_\nu(z) \equiv \int_0^\infty \frac{x^\nu}{\exp(x-z)+1}\, dx \tag{8}$$

is the Fermi integral. With the use of Padé approximants to the functions $I_\nu(z)$ and their inverse functions [37], $F_{\rm id}^{(e)}$ is expressed as an analytic function of N_e, V, and T.

In the zero-temperature limit, one may replace $I_\nu(\beta\mu_e)$ by $(\beta\epsilon_F)^{\nu+1}/(\nu+1)$, which gives, in particular, the well-known expression

$$\epsilon_F = \frac{\hbar^2}{2m_e}(3\pi^2 n_e)^{2/3}. \tag{9}$$

The Fermi temperature is defined as $T_F \equiv \epsilon_F/k_B \approx 3\times 10^5 \hat{\rho}^{2/3}$ K, where $\hat{\rho} = 1.6735 n_e/(10^{24}\,{\rm cm}^{-3})$ is the mass density of the electron-proton plasma in g cm^{-3}. In the nondegenerate limit $T \gg T_F$, the ideal Boltzmann gas relations are recovered, $\mu_e = k_B T \ln(n_e\lambda_e^3/2)$ and $P_e = n_e k_B T$.

For the atoms, one has

$$F_{\rm id}^{\rm H} = k_B T \sum_\kappa N_\kappa [\ln(n_\kappa \lambda_{\rm H}^3/g_\kappa) - 1 - \beta\chi_\kappa], \tag{10}$$

where κ enumerates quantum states with statistical weights g_κ and binding energies χ_κ.

It should be noted that, although nonideality effects are not included in $F_{\rm id}$ explicitly, they do affect the equilibrium value of $F_{\rm id}$ through particle numbers. In particular, the distribution of N_κ in Eq. (10) is *not* assumed to obey the ideal-gas Boltzmann law.

Finally, the radiation term (which can be important only at low ρ or very high T) reads

$$F_{\rm rad} = -(4\sigma/3c) V T^4, \tag{11}$$

where $\sigma = \pi^2 k_B^4/(60\hbar^3 c^2)$ is the Stefan-Boltzmann constant.

2. Excess free energy

The excess free energy is conventionally written as

$$F_{\rm ex} = F_{\rm ex}^C + F_{\rm ex}^{\rm neu}, \tag{12}$$

where $F_{\rm ex}^C$ is the excess free energy of the ionized part of the plasma and $F_{\rm ex}^{\rm neu}$ accounts for interactions of neutral species with electrons, protons, and other neutral species. The Coulomb term

$$F_{\rm ex}^C = F_{ii} + F_{ee} + F_{ie} \tag{13}$$

includes contributions from the exchange and correlation interactions of electrons F_{ee}, Coulomb interactions in the one-component plasma (OCP) of ions F_{ii}, and ion-electron (screening) interaction F_{ie}. These contributions have been calculated by various procedures, e.g., by solving a set of hypernetted-chain equations or Monte Carlo simulations [38–42]. We make use of the fitting formulas to the results of such calculations, obtained in [39] for F_{ee} and in [41] for F_{ii} and F_{ie}. These formulas express the electron-ion plasma free energy as an analytic function of the electron density parameter

$$r_s = a_e/a_0 \approx 1.39\hat{\rho}^{-1/3} \tag{14}$$

and Coulomb coupling parameter

$$\Gamma = \beta e^2/a_e \approx 0.227\hat{\rho}^{1/3}/T_6, \tag{15}$$

where $a_e = (4\pi n_e/3)^{-1/3}$ is the mean interelectron distance and $T_6 \equiv T/10^6$ K.

The nonideal part of the atomic free energy, $F_{\rm ex}^{\rm neu}$, can be written as [33,34]

$$F_{\rm ex}^{\rm neu} = F_{\rm HS} + F_{\rm pert}, \tag{16}$$

where $F_{\rm HS}$ is the reference free energy, treated in the hard-sphere approximation, and $F_{\rm pert}$ is the perturbation part that accounts for the attractive (van der Waals) interactions. To calculate these contributions, an elaborate model has been developed by SC [33,34]. Its simplified analytic version for weak electron degeneracy has been constructed in [32]. In the so-called van der Waals one-fluid model [43], a free energy of the hard-sphere mixture is represented by the Carnahan-Starling formula [44]

$$\beta F_{\rm HS}/N_{\rm tot} = (4\eta - 3\eta^2)/(1-\eta)^2, \tag{17}$$

where $N_{\rm tot} = \Sigma_\alpha N_\alpha$ is the total number of particles,

$$\eta = \frac{\pi}{6N_{\rm tot}V} \sum_{\alpha\alpha'} N_\alpha N_{\alpha'} d_{\alpha\alpha'}^3, \tag{18}$$

is the effective packing fraction, and $d_{\alpha\alpha'}$ are the hard-sphere interaction diameters. In our case, the subscript α enumerates atomic quantum states described by quantum numbers κ and takes on a single value p for the free protons.

In the following, we compare two versions of the model: (i) the *full* version, in which $F_{\rm pert}$ and $d_{\alpha\alpha'}$ are given by approximations of [32], with one exception (adopted from [34]) that $d_{\alpha\alpha'}$ cannot be smaller than a certain limit $d_{\alpha\alpha'}^{(0)}$, and (ii) the *simple* version, in which long-range atomic interactions are disregarded. In the latter case, $F_{\rm pert} = 0$ and $d_{\alpha\alpha'} = d_{\alpha\alpha'}^{(0)}$. Furthermore, we adopt the simplest choice

$$d_{\kappa\kappa'}^{(0)} = l_\kappa + l_{\kappa'}, \quad d_{\kappa p}^{(0)} = l_\kappa, \tag{19}$$

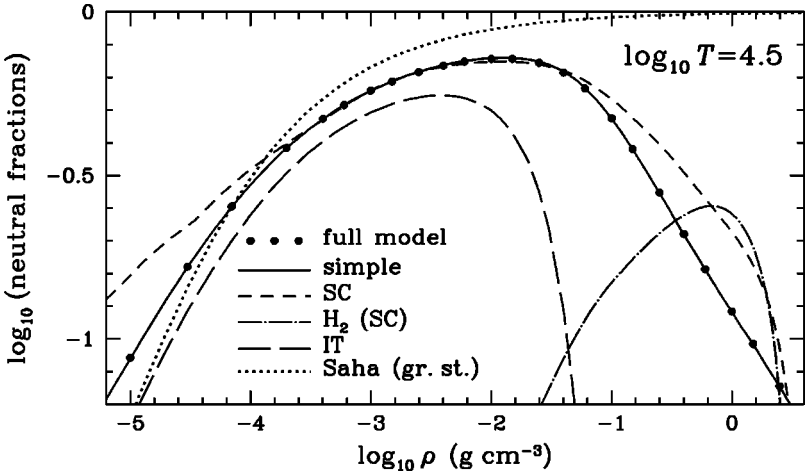

FIG. 1. Comparison of the fraction of neutral atoms $f_{\rm H}=n_{\rm H}/n_0$ given by SC tables (short-dashed line) and by two present versions of the thermodynamic model of partially ionized atomic hydrogen (see text). The long-dashed line corresponds to the fraction of atoms that satisfy the Inglis-Teller criterion. The dotted line is given by the usual Saha equation for ground-state atoms.

where l_κ is the root-mean-square proton-electron distance in the quantum state κ [45]. For the interactions among charged particles, we define $d_{\alpha\alpha'}=0$, because this type of interaction is already included in the Coulomb part of the free energy. Note that in the second (simple) version of the model, $F_{\rm HS}$ turns into the unbinding term F_{ub} of Ref. [32] in the low-density limit ($\eta\ll 1$). Thus the unbinding term is now incorporated in $F_{\rm HS}$, which allows us to approximately take into account the correlation effects.

C. Equilibrium conditions

Thermodynamic equilibrium is given by the minimization of $F(V,T,\{N_\alpha\})$ with respect to the particle numbers N_α under stoichiometric constraints. The condition of the extremum of F can be written in the form of the Saha equation corrected for nonideality and electron degeneracy:

$$n_{\rm H}=n_p n_e \lambda_e^3 (m_p/m_{\rm H})^{3/2}(Z_w/2)e^{\Lambda}, \tag{20}$$

where

$$\Lambda=\beta\partial F_{\rm id}^{(e)}/\partial N_e-\ln(n_e\lambda_e^3/2) \tag{21}$$

allows for electron degeneracy and

$$Z_w=\sum_\kappa g_\kappa w_\kappa e^{\beta\chi_\kappa} \tag{22}$$

is the modified IPF which includes the occupation probabilities w_κ, defined according to [32]:

$$k_B T\ln w_\kappa=\frac{\partial F_{\rm ex}}{\partial N_p}+\frac{\partial F_{\rm ex}}{\partial N_e}-\frac{\partial F_{\rm ex}}{\partial N_\kappa}. \tag{23}$$

To solve Eq. (20), one must add the electroneutrality condition $n_e=n_p$ and the mass conservation condition $n_{\rm H}+n_p=n_0$, where $n_0=\rho/m_{\rm H}=(\rho/11.293\,{\rm g\,cm^{-3}})a_0^{-3}$.

The Boltzmann distribution of the atoms, corrected for nonideality, reads

$$n_\kappa=n_{\rm H} g_\kappa w_\kappa e^{\beta\chi_\kappa}/Z_w. \tag{24}$$

The minimum of the free energy is sought by solving Eqs. (20)–(24) iteratively [32]. First, one defines starting w_κ's and calculates the number densities from Eqs. (20) and (24). Then the w_κ's are refined using these number densities in Eq. (23) [46].

The molecules H_2 can be easily included in this procedure. The dissociation-recombination equation reads

$$n_{\rm H_2}=n_{\rm H}^2(\lambda_{\rm H}\sqrt{2})^3 Z_{w2}/Z_w^2, \tag{25}$$

where Z_{w2} is the molecular IPF, modified by multiplying each κth term by an occupation probability $w_\kappa^{\rm H_2}$ [32], given by

$$k_B T\ln w_k^{\rm H_2}=2\left(\frac{\partial F_{\rm ex}}{\partial N_p}+\frac{\partial F_{\rm ex}}{\partial N_e}\right)-\frac{\partial F_{\rm ex}}{\partial N_\kappa^{\rm H_2}}. \tag{26}$$

For simplicity, we do not include molecules in the present versions of the model, because the fraction of H_2 is small in the range of ρ and T which we are interested in.

After the equilibrium distribution of plasma particles is found, the pressure P, internal energy U, and entropy S are calculated from the relations

$$P=-(\partial F/\partial V)_{T,\{N_\alpha\}},\quad U=[\partial(\beta F)/\partial\beta]_{V,\{N_\alpha\}}, \tag{27}$$

$S=(U-F)/T$. The higher-order thermodynamic quantities are obtained by differentiation of P,U,S without keeping N_α fixed [36].

D. Results of comparison

The ionization curves given by different versions of the model are compared in Fig. 1 for $T=10^{4.5}$ K. Although the neglect of the perturbation terms introduced in the simple version is most perceptible at such relatively low temperatures, the ''full'' and ''simple'' versions of the model yield practically identical atomic fractions $f_{\rm H}\equiv n_{\rm H}/n_0$.

The results of SC [31] qualitatively agree with the present model. Quantitatively, they differ in the pressure-ionization region at $\rho>0.1\,{\rm g\,cm^{-3}}$, where the theoretical uncertainty is largest (see Sec. IIA). The difference in the low-density regime $\rho<10^{-4}\,{\rm g\,cm^{-3}}$ is due to highly excited states. If both the effective diameter d and statistical weight g_n are proportional to n^2 (n being the principal quantum number), then the neutral fraction should asymptotically decrease at low density as $f_{\rm H}\propto\rho^{1/2}$. Our present model exhibits this asymptotic

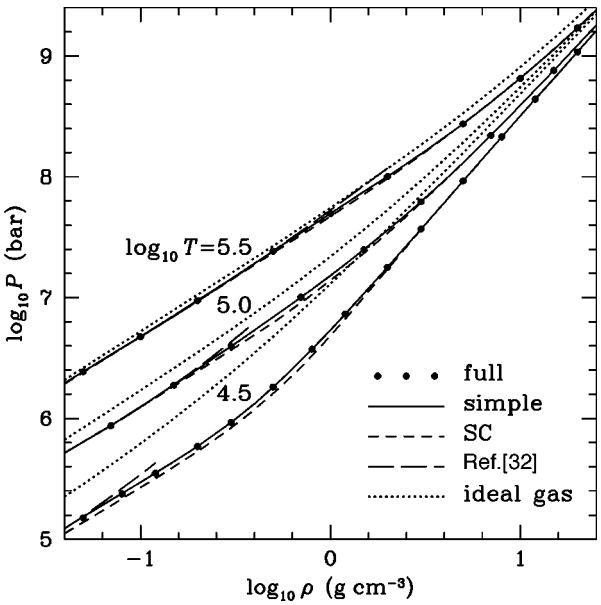

FIG. 2. Comparison of two present versions of the EOS of partially ionized atomic hydrogen (see text) with Refs. [31] (SC) and [32]. The EOS of ideal fully ionized gas is also shown.

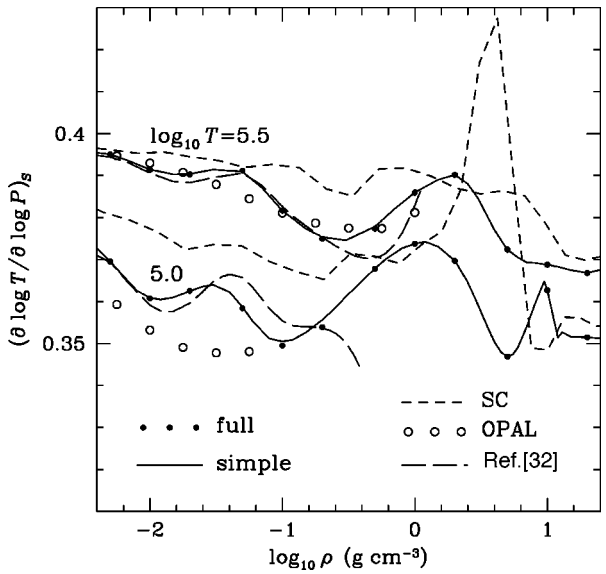

FIG. 3. Two adiabatic gradient isotherms given by different EOS models in the domain of partially ionized atomic hydrogen.

behavior; the dependence $f_{\mathrm{H}} \propto \rho^{1/3}$ seen at low ρ in the SC data might result from a choice $d \propto n$.

The long-dashed curve represents the fraction of atoms satisfying the Inglis-Teller criterion: $f_{\mathrm{IT}} = \Sigma n_\kappa \tilde{w}_\kappa / n_0$. Here, $\tilde{w}_\kappa$ is the probability that a given atom is not strongly perturbed by plasma microfields; it is estimated from Eq. (31) of Ref. [32]. Using f_{IT}, we have calculated monochromatic opacities of the plasma and compared them with the OPAL monochromatic opacities [47] (at $\rho \leqslant 10 T_6^3\ \mathrm{g\,cm^{-3}}$ where the OPAL data exist). Along the isotherm shown in Fig. 1, our results agree with OPAL within 12% in the photon energy range from 13.6 eV to 500 eV where the opacity is dominated by bound-free atomic absorption. For comparison, hydrogen opacities calculated in [48] differ from OPAL by up to 37% (in the same range of energy and density at the same T).

Figure 2 demonstrates that the EOSs obtained with the full and simple versions of our model practically coincide. In the region of weak degeneracy, they also coincide with the model presented in [32]. Moreover, there is a good agreement with the SC model [31]. Small differences occur only in the regions where the SC model predicts an appreciable amount of molecules, as explained in [32].

As is well known, the second-order quantities are more sensitive to the details of the thermodynamic model than the first-order ones. The adiabatic temperature gradient

$$\nabla_{\mathrm{ad}} = (\partial \ln T / \partial \ln P)_S \tag{28}$$

is shown in Fig. 3. There are only tiny differences between the full and simple versions. For comparison, we also show ∇_{ad} from other models. In its validity region (i.e., at low density), the model [32] approximately agrees with the present one. The differences with predictions of SC are somewhat larger. In all models, the isotherms ''wiggle'' in the region of consecutive pressure destruction of excited atomic states. Such wiggles are absent in the OPAL data [49], based on the physical picture of the plasma and also shown in Fig. 3. Compared to SC, the present data tend to be closer to the OPAL data. We conclude that the simplifications introduced above are acceptable to describe the thermodynamics of atomic hydrogen. In Sec. IV, we generalize the model to the case of the strong magnetic field.

III. FULLY IONIZED PLASMA IN A STRONG MAGNETIC FIELD

In this section, we describe effects of quantizing magnetic fields on the fully ionized proton-electron plasma. We assume that the field **B** is uniform and directed along the z axis.

A. Ideal gas

1. Electrons

The electron energy in a magnetic field reads [50]

$$\epsilon_N(p_z) = N\hbar\omega_c + p_z^2/(2m_e), \tag{29}$$

where p_z is the longitudinal momentum and $N = 0,1,2\ldots$ is the Landau quantum number. All levels except the lowest one are double degenerate with respect to the spin projection. Strictly speaking, the anomalous magnetic moment of an electron leads to a splitting of the levels $N \geqslant 1$ by $0.001\,16\hbar\omega_c$, which takes off the double degeneracy. However, this splitting cannot affect the thermodynamics at $\rho < \rho_B$, where $k_B T$ should be at least comparable to $\hbar\omega_c$ for an appreciable population of the excited Landau levels.

The thermodynamic functions of the electron gas in the magnetic field are easily derived from the first principles [36]. Taking into account the fact that the number of quantum states of an electron with fixed discrete quantum numbers in volume V per longitudinal momentum interval Δp_z equals $V\Delta p_z/(4\pi^2 a_m^2 \hbar)$ [50], the thermodynamic potential $\Omega = -PV$ can be written as

$$\Omega = -\frac{Vk_BT}{2\pi^2 a_m^2 \hbar}\sum_{N=0}^{\infty} g_N \int_0^{\infty} \ln(1+e^{\beta[\mu_e-\epsilon_N(p_z)]})dp_z,$$

where g_N is the statistical weight ($g_0=1$ and $g_N=2$ for $N \geqslant 1$). Hence the electron pressure and number density are given by the equations

$$P_e = \frac{k_BT}{\pi^{3/2}a_m^2\lambda_e}\sum_{N=0}^{\infty} g_N I_{1/2}(\beta\mu_N), \tag{30}$$

$$n_e = \frac{1}{2\pi^{3/2}a_m^2\lambda_e}\sum_{N=0}^{\infty} g_N I_{-1/2}(\beta\mu_N), \tag{31}$$

where $\mu_N \equiv \mu_e - N\hbar\omega_c$. The Helmholtz free energy is given by Eq. (5), where μ_e can be found by inversion of Eq. (31) (e.g., using an algorithm described in [51]).

In the nonquantizing magnetic field $T_B \ll T$, where many Landau levels are populated, the sum over N in Eqs. (30), (31) may be approximated by an integral, and integration by parts reproduces Eqs. (6), (7).

In the domain of strong magnetic quantization, $T \ll T_B$ and $\rho < \rho_B$, one may retain only the term $N=0$. In that case, replacing $I_{-1/2}(\beta\mu_e)$ by $2\sqrt{\beta\epsilon_F}$ in Eq. (31) (by analogy with Sec. II B) yields the Fermi energy

$$\epsilon_F = \frac{2\pi^4\hbar^2}{m_e}(a_m^2 n_e)^2. \tag{32}$$

By definition, $\rho=\rho_B$ at $\epsilon_F=\hbar\omega_c$. Hence $\rho/\rho_B = 3\pi(2\gamma r_s^2)^{-3/2}$, from which Eq. (1) follows. A comparison of Eqs. (9) and (32) reveals that the Fermi energy changes by a factor $(4/3)^{2/3}(\rho/\rho_B)^{4/3}$. Thus the degeneracy is strongly reduced at $\rho \ll \rho_B$.

In the nondegenerate regime $T \gg T_F$, one has $I_\nu(\beta\mu_e) \approx \exp(\beta\mu_e)\Gamma(\nu+1)$; therefore Eqs. (30), (31) reduce to $P_e = n_e k_B T$ and

$$\beta\mu_e = \ln(n_e\lambda_e^3/2) - \ln u + \ln(\tanh u), \tag{33}$$

where $u \equiv \beta\hbar\omega_c/2 = T_B/(2T)$. This yields an explicit analytic form for $F_{\rm id}^{(e)}$. In the nonquantizing field, $T_B \ll T$, the last two terms in Eq. (33) cancel out, and the classical expression (Sec. II B) is recovered. In the strongly quantizing regime $\rho < \rho_B$ and $T_F \ll T \ll T_B$, the last term of Eq. (33) vanishes, which yields

$$F_{\rm id}^{(e)} = N_e k_B T[\ln(2\pi a_m^2\lambda_e n_e) - 1]. \tag{34}$$

2. Protons

The transverse motion of protons is quantized in Landau orbitals with the elementary excitation equal to the proton cyclotron energy $\hbar\omega_{cp} = (m_e/m_p)\hbar\omega_c$. The energy spectrum is given by Eq. (29) when replacing m_e by m_p and ω_c by ω_{cp}. Unlike the case of electrons, the double-spin degeneracy of the Landau levels is taken off by the abnormal magnetic moment of the proton.

In our analysis, the protons are always nondegenerate, so that by analogy with Eq. (34) we have

$$\beta F_{\rm id}^{(p)}/N_p = \ln(2\pi a_m^2\lambda_p n_p) + \ln[1-e^{-\beta\hbar\omega_{cp}}] - 1. \tag{35}$$

Here, for sake of brevity, we drop the zero-point energy $\frac{1}{2}\hbar\omega_{cp}$ and the spin energy $\pm\frac{1}{4}g_p\hbar\omega_{cp}$, where $g_p=5.585$ is the proton spin gyromagnetic factor [50]. We suppress these terms also for atoms and molecules. Taking them into account yields an additive contribution to the total free energy of the system, equal to

$$\Delta F = N_0\left\{\frac{1}{2}\hbar\omega_{cp} - k_BT\ln[2\cosh(\beta g_p\hbar\omega_{cp}/4)]\right\} \tag{36}$$

($N_0=N_p$ in the case of full ionization). Since N_0 is constant, ΔF affects neither ionization equilibrium nor pressure, but it does affect the internal energy and specific heat; therefore we take it into account in Sec. V.

B. Nonideal Coulomb plasma

According to the Bohr–van Leeuwen theorem, a magnetic field does not affect the thermodynamics of classical charged particle systems (see, e.g., Ref. [52]). Thus the classical ionic OCP excess free energy $F_{ii}(\Gamma)$ does not depend on B at any Γ. The classical regime for the electron-proton plasma corresponds to $r_s \gg 1$ and $\Gamma \ll 1$, where the excess Coulomb free energy is given by the Debye-Hückel formula $F_{\rm ex}^C = -N_e k_B T\sqrt{8\Gamma^3/3}$. Indeed, it is easy to check that this law holds independent of B [8].

A magnetic field, however, affects quantum-mechanical contributions to $F_{\rm ex}^C$. These effects have been studied only in low-temperature or low-density regimes.

The ground-state exchange energy of the electron gas in the strongly quantizing field [7,53] behaves as $-2.25(\gamma r_s^3)^{-1}[\ln(\gamma r_s^2) - 0.457 + \cdots]e^2/a_0$ (per electron), compared to $-0.75\pi^{-1}(9\pi/4)^{1/3}r_s^{-1}e^2/a_0$ in the nonmagnetic case [54]. Thus the exchange energy at $T \ll T_F$ is suppressed by a factor $\approx 0.2036\gamma r_s^2/[\ln(\gamma r_s^2) - 0.457]$. Note that the condition of strong magnetic quantization requires γr_s^2 to be large.

A general low-density expansion for the free energy of a Coulomb plasma in an arbitrary magnetic field up to order $\rho^{5/2}$ has been derived by Cornu [52]. The coefficients of this expansion are not available in explicit analytic form but require numerical evaluation, which has not been done yet. In the particular case of the OCP, a Wigner-Kirkwood-type expansion in powers of $\hbar$ is available [52]. The lowest-order term of the latter expansion (quantum diffraction term of order $\hbar^2$) has been obtained by Alastuey and Jancovici [55]:

$$F_{\rm diff} = N_e k_B T\frac{\Gamma^2}{8r_s}\left[\frac{2}{u\tanh u} - \frac{2}{u^2} + \frac{1}{3}\right], \tag{37}$$

with u defined as in Eq. (33). The square brackets in Eq. (37) go to 1 at $u \to 0$, recovering the well-known zero-field result, and to 1/3 at $u \gg 1$, reflecting the fact that two of three degrees of freedom for the electron motion are frozen out in the strongly quantizing field. Equation (37) is valid in the low-density regime, where $r_s \gg \max(\Gamma, \Gamma^{-1})$. In this regime the correction (37) is smaller than the classical OCP corrections to the Debye-Hückel formula. In the electron-ion plasmas, $F_{\rm diff}$ is canceled because of the local neutrality relation [52].

In this paper, we are mainly interested in the case where $(\Gamma r_s)^{-1} \approx 3.16T_6 \gtrsim 1$. In this case, a high-temperature expan-

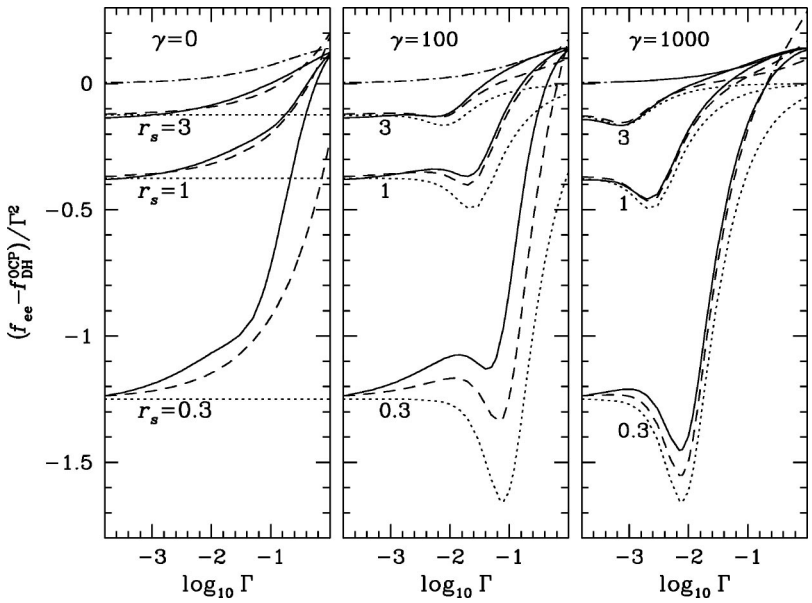

FIG. 4. Contribution to the electron-gas nonideal free energy $f_{ee}=\beta F_{ee}/N_e$ beyond $f_{\rm DH}^{\rm OCP}=-\Gamma^{3/2}/\sqrt{3}$ at three values of the magnetic field parameter γ and three values of the density parameter r_s (indicated). The scaled fit (solid lines; see text) is compared with the high-temperature expansion up to orders e^2 and e^4 (dotted and dashed lines, respectively) and with the classical OCP (dot-dashed lines).

sion [56], which can be written as an expansion in powers of two small parameters $s_1=\sqrt{\Gamma}/r_s$ and $s_2=\sqrt{\Gamma}/r_s$, is relevant at low densities. The lowest-order correction is the Hartree-Fock term $\propto\hbar^2e^2$. Steinberg *et al.* [21] have recently obtained an analytic result for this term in a magnetic field:

$$\frac{\beta F_{\rm HF}}{N_e}=-\frac{3\Gamma^2}{8r_s}f_1(u), \tag{38}$$

where the function

$$f_1(u)=\frac{\cosh(2u)}{\cosh^2 u}\left[\frac{\tanh u}{u}\right]\frac{\operatorname{arctanh}(\sqrt{1-u^{-1}\tanh u})}{\sqrt{1-u^{-1}\tanh u}} \tag{39}$$

goes to 1 at small u, reproducing the zero-field result [56], and to $\ln(4u)/u$ at very large u.

Steinberg *et al.* [21] have also calculated the corrections $\propto\hbar e^4$ (the Montroll-Ward and exchange terms). For the electron gas, they can be written in the form

$$\frac{\beta F_4}{N_e}=\frac{3\sqrt{\pi}}{16}\frac{\Gamma^{5/2}}{\sqrt{r_s}}[f_2^{ee}(u)+f_3^{ee}(u)\ln 2], \tag{40}$$

where $f_2^{ee}(u)$ and $f_3^{ee}(u)$ go to 1 at $u\to 0$, reproducing the zero-field result [56], and decrease at large u.

In order to incorporate these results into the analytic free-energy model, we employ a simple scaling procedure. In the fit for $f_{ee}(\theta,\Gamma)=\beta F_{ee}/N_e$ derived in [39], where $\theta=T/T_F$ is the degeneracy parameter, we replace the zero-field value $\theta_0=2(9\pi/4)^{-2/3}r_s/\Gamma$ by

$$\theta^*=\theta_0\frac{1+\theta_m/\theta_0}{1+f_1(u)(\theta_m/\theta_0)\exp(-\theta_m^{-1})}. \tag{41}$$

Here, $\theta_m=8\gamma^2r_s^5/(9\pi^2\Gamma)=0.166\theta_0\gamma^2r_s^4$ is the value of the degeneracy parameter in the strongly quantizing field.

The scaling (41) reproduces limiting cases: (i) at $r_s\gg 1$, the classical OCP expression is recovered, independently of other parameters; (ii) in the nonquantizing regime $\gamma r_s^2\ll 1$, we get the nonmagnetic value $\theta^*=\theta_0$; (iii) in the strongly quantizing degenerate regime $\gamma r_s^2\gg 1$ and $\theta_m\ll 1$, the correct value of the degeneracy parameter $\theta^*=\theta_m$ is recovered; and (iv) in the strongly quantizing nondegenerate regime $\gamma r_s^2\gg 1$ and $\theta_m\gg 1$, the fit reproduces Eq. (38) in its range of validity.

Figure 4 demonstrates the validity of the adopted modification of F_{ee} at $\Gamma<1$, for three values of r_s, for which the quantum contributions to $F_{\rm ex}^C$ could appreciably affect our results. We plot *departures* of F_{ee} from the OCP Debye-Hückel function $F_{\rm DH}^{\rm OCP}$, normalized to N_ek_BT and divided for convenience by Γ^2. The dot-dashed line shows the classical OCP free energy [41], the dotted line displays the e^2 correction (38), and the dashed line results from inclusion of the e^4 corrections (40).

The left panel presents the nonmagnetic case. The solid line shows the fit to F_{ee} [39]. The region of approximate coincidence of the fit with the high-T expansion can be adopted as the region of validity of the latter. At large r_s, it is restricted by the condition $s_2\ll 1(\Gamma\ll r_s^{-1})$, while at small r_s, the condition $s_1\ll 1(\Gamma\ll r_s^2)$ is more restrictive.

The middle and right panels show the modifications of F_{ee} at two values of the magnetic field strength. One can see that the scaled fit satisfactorily reproduces the expansion in the validity range of the latter. Surprisingly, although the scaling is based on the lowest-order e^2 term (38), the e^4 terms (40) are also well reproduced.

For the electron-ion plasma, the screening contribution F_{ie} should be taken into account. At $B=0$, it has been calculated in a number of papers (e.g., Refs. [39–41]) and fitted by analytic expressions [41]. In a strongly quantizing magnetic field, this contribution has been analytically evaluated only for a dense plasma at zero temperature using the linear response theory [7]. Comparison with the analogous zero-field result [57] shows that the strongly quantizing magnetic field increases the screening energy at high density by factor $0.8846\gamma^2r_s^4$. To our knowledge, there were no relevant calculations at arbitrary degeneracy. In the regime of low degeneracy and weak Coulomb coupling, integral representations of the low-density expansion coefficients have been

obtained [21,52]. The contribution of order e^4 is given by Eqs. (20), (21) of Ref. [21]. It is reproduced if to replace r_s by $r_s/(f_2^{ep})^2$ in the nonmagnetic expression [56]. Here, f_2^{ep} can be approximated (within 0.5%) as

$$f_2^{ep}=\frac{1}{2}+t^{0.9}\frac{\operatorname{arctanh}[(1-t)^{0.6}]}{2(1-t)^{0.6}}, \tag{42}$$

where $t\equiv\tanh(0.4u)/(0.4u)$. We apply the scaling $r_s \to r_s/(f_2^{ep})^2$ to the formula for $F_{ie}(r_s,\Gamma)$ given in [41].

IV. PARTIALLY IONIZED PLASMA

A. Hydrogen bound species in the strong magnetic field

1. Atoms

Only a brief summary of the properties of the hydrogen atom in a strong magnetic field is given below. See, e.g., Ref. [17] for details and references.

The motion of an atom in a magnetic field **B** can be conveniently described using the pseudomomentum **K**, the quantum-mechanical constant of motion related to the average center-of-mass velocity $\mathbf{v}=\boldsymbol{\nabla}_{\mathbf{K}}E$, where E is the total energy of the atom. If there were no Coulomb attraction, the energy would be $E=E_{Ns}^{\perp}+K_z^2/(2m_{\rm H})$, where

$$E_{Ns}^{\perp}=N\hbar\omega_c+(N+s)\hbar\omega_{cp} \tag{43}$$

is the energy of the transverse excitation, N is the electron Landau number, s is the z projection of the relative proton-electron angular momentum, and $K_z^2/(2m_{\rm H})$ is the kinetic energy of motion along the field. The Coulomb interaction mixes the Landau orbitals. Nevertheless, it is convenient to keep the quantum numbers N and s for enumerating the quantum states at $\gamma\gg1$. Then the energy of the atom can be decomposed as follows:

$$E_{Ns\nu}(\mathbf{K})=E_{Ns\nu}^{\parallel}(K_\perp)+E_{Ns}^{\perp}+K_z^2/(2m_{\rm H}), \tag{44}$$

where $E_{Ns\nu}^{\parallel}(K_\perp)<0$ is the ''longitudinal'' energy, and the quantum number ν enumerates the longitudinal excitations. At $\gamma\gg1$, the states with $N\neq0$ or large s are subject to autoionization. Therefore we put $N=0$ and suppress this quantum number hereafter. The binding energy is

$$\chi_{s\nu}(K_\perp)=|E_{s\nu}^{\parallel}(K_\perp)|-s\hbar\omega_{cp}. \tag{45}$$

In accordance with Sec. III A 2, the zero-point and spin terms are subtracted from Eq. (43) and absorbed into Eq. (36). Note that Eq. (36) is valid for the partially ionized plasma provided that the IPF's for atoms with opposite proton spin projections are identical. It is true under the assumption that the autoionization processes with proton spin flip may be neglected on the plasma relaxation time scale. We adopt this assumption, because the plasma under consideration is rather dense and nonrelativistic. Otherwise, states with binding energy $\chi_{s\nu}(K_\perp)<g_p\hbar\omega_{cp}/2$ should be excluded from the IPF for atoms with the negative proton spin projection.

At $K=0$, the atom is axially symmetric, and its sizes transverse to the magnetic field can be approximated [1,24] as $l_x=l_y\approx a_m\sqrt{s+1}$, while the longitudinal size is much larger: $l_z\sim a_0/\ln\gamma$ for the *tightly bound* states ($\nu=0$) and $l_z\sim a_0\nu^2$ for the *hydrogenlike* states ($\nu\geqslant1$). Longitudinal energies of the former states grow as $E^{\parallel}\propto(\ln\gamma)^2$, whereas the energies of the latter states are relatively small, $|E^{\parallel}| \sim(e^2/a_0)(2n^2)^{-1}$, where n is the integer part of $(\nu+1)/2$.

An atom moving across the field acquires a constant dipole moment in the direction opposite to its *guiding center* $\mathbf{r}_c=c(eB^2)^{-1}\mathbf{B}\times\mathbf{K}$. When $K_\perp$ is small enough, the dipole moment is also small, and $E^{\parallel}$ is increased by $K_\perp^2/(2m_{s\nu}^{\perp})$. Here, $m_{s\nu}^{\perp}$ is the so-called *effective transverse mass*, which exceeds $m_{\rm H}$ and grows with field strength. In this case the average transverse velocity is $v_\perp=K_\perp/m_{s\nu}^{\perp}$. When $K_\perp$ exceeds some critical value $K_c\sim10^2\hbar/a_0$, the atom becomes *decentered*: $v_\perp$ reaches a maximum and starts to decrease, while the electron-proton separation approaches r_c. Thus, for the decentered states, the transverse pseudomomentum $K_\perp$ characterizes electron-proton separation rather than velocity.

In the limiting case of $K_\perp\gg\gamma(\nu+1/2)^2\hbar/a_0$, the longitudinal energies approach the asymptote $E^{\parallel}\sim-e^2/r_c$. Note that only the states with $s=0$ may remain bound if they have such large values of $K_\perp$. Indeed, since $E^{\parallel}$ is small for large $K_\perp$, the binding energy (45) becomes negative for $s\geqslant1$. However, at $s=0$ and arbitrarily large $K_\perp$, there still remains an infinite number of truly bound states (enumerated by ν), as has been strictly proved in [17].

Since $r_c=a_0^2K_\perp/\gamma\hbar$, the decentered states have huge sizes at $\gamma<1$; hence they are expected to be destroyed by collisions with surrounding particles in the laboratory and in white-dwarf atmospheres [58]. In neutron-star atmospheres at $\gamma\gtrsim10^3$, however, the decentered states may be significantly populated, as we shall see below.

Accurate numerical dependences of the atomic binding energies $\chi_{s\nu}(K_\perp)$ and sizes $l_{s\nu}(K_\perp)$ for $300\leqslant\gamma\leqslant10^4$ and any $K_\perp$ have been obtained in [17,24]. In Ref. [24], analytic fits have been constructed for these quantities as functions of γ and $K_\perp$, as well as for the critical pseudomomentum K_c and transverse mass $m_{s\nu}^{\perp}$ as functions of γ, for various s and ν. These fits are more suitable for studying the thermodynamics of hot plasmas than previous approximations [19], which were accurate only for the centered ground state ($s=\nu=0$ and $K_\perp<K_c$).

2. Other bound species

At sufficiently low T or high B, there may exist a considerable amount of molecules and ions in the hydrogen plasma. The molecular ion H_2^+ has been thoroughly investigated at $B<10^{10}$ G, including the dependence of binding energies of various electron-vibrational-rotational levels on the angle between the ion axis and the magnetic field direction [59]. For stronger fields, only the parallel configuration has been considered [12,60–62]. The ions H_2^+ have negligible abundance in the strong field, owing to the small binding energy, compared to the atoms and H_2 molecules [12,20]. The same is probably true for H^- ions [20].

H_2 molecules have been studied in detail at various field strengths [60,61,63]. An interesting result is that the ground state is unbound at $0.18<\gamma<12.3$ [63]. Fitting formulas for the dissociation energies in the parallel configuration for $\gamma\gtrsim10^3$ have been given in [20,61]. At such fields, the disso-

ciation energy grows $\propto(\ln\gamma)^2$, approximately at the same rate as the atomic ground-state energy. The equilibrium internuclear distance decreases as $1/\ln\gamma$, being as small as $1/4a_0$ at $B=10^{12}$ G, again roughly proportional to the longitudinal size of the atom.

Moreover, strong magnetic fields stabilize polymer chains H_N aligned with **B**, as first suggested by Ruderman [64] and later confirmed by Hartree-Fock calculations [60]. The specific quantum-mechanical properties of these species (e.g., their excitation spectra) are poorly known.

Motional effects on the molecules and chains in the strong magnetic fields have not been studied. Therefore, one cannot construct a reliable EOS in the domain of ρ,T,B where these species are expected to dominate. For instance, Lai and Salpeter [20] estimated the effective transverse mass of H_N as N times the atomic effective mass, $Nm_{00}^{\perp}$, and used it in the dissociation equilibrium equation. However, since the heavier molecule has lower velocity at a given K, it is exposed to a weaker electric field in the comoving frame. Therefore, one could expect its energy levels to be less perturbed and its effective mass to be closer to the zero-field value, $Nm_{\rm H}$.

Because of these uncertainties, we do not include H_N in our study but restrict ourselves to the atomic phase. Nevertheless, we include ground-state H_2 molecules in order to determine the validity domain of our results.

B. Free-energy model

Our free-energy model is a straightforward generalization to the magnetic case of the model presented in Sec. II B:

$$F=F_{\rm id}^{(e)}+F_{\rm id}^{(p)}+F_{\rm id}^{\rm neu}+F_{\rm rad}+F_{\rm ex}^{C}+F_{\rm ex}^{\rm neu}. \tag{46}$$

The ideal electron and proton free energies $F_{\rm id}^{(e)}$ and $F_{\rm id}^{(p)}$ are derived in Secs. III A 1 and III A 2, respectively. $F_{\rm rad}$ is given by Eq. (11). The Coulomb part $F_{\rm ex}^{C}$ has been discussed in Sec. III B. Now let us consider the ideal and nonideal contributions $F_{\rm id}^{\rm neu}$ and $F_{\rm ex}^{\rm neu}$ brought about by the bound species.

Since the quantum-mechanical characteristics of an atom in a strong magnetic field depend in a nontrivial way on the transverse pseudomomentum $K_\perp$, the distribution of atoms over $K_\perp$ cannot be written in a closed form, and only the distribution over K_z remains Maxwellian. Let $p_{s\nu}(K_\perp)d^2K_\perp$ be the probability to find an atom with given (s,ν) in an element $d^2K_\perp$ near the point $\mathbf{K}_\perp$ of the transverse pseudomomentum plane. For the Maxwell distribution, we would have $p_{s\nu}(K_\perp)=(2\pi\hbar)^{-2}\lambda_{\rm H}^2\exp[-K_\perp^2/(2m_{\rm H})]$. In the general case, the number of atoms in an element d^3K of the pseudomomentum space is

$$dN(\mathbf{K})=N_{s\nu}\frac{\lambda_{\rm H}}{2\pi\hbar}\exp\left(-\frac{\beta K_z^2}{2m_{\rm H}}\right)p_{s\nu}(K_\perp)d^3K, \tag{47}$$

where $N_{s\nu}=\int dN_{s\nu}(\mathbf{K})$ is the total number of atoms with the specified discrete quantum numbers. The distribution $N_{s\nu}p_{s\nu}(K_\perp)$ is not given in advance but should be calculated self-consistently by minimization of the total free energy, including nonideal terms.

It is convenient to introduce deviations from the Maxwell-Boltzmann distribution through the occupation probabilities $w_{s\nu}(K_\perp)$:

$$p_{s\nu}(K_\perp)=\left(\frac{\lambda_{\rm H}}{2\pi\hbar}\right)^2\frac{w_{s\nu}(K_\perp)\exp[\beta\chi_{s\nu}(K_\perp)]}{Z_{s\nu}}, \tag{48}$$

$$N_{s\nu}/N_{\rm H}=Z_{s\nu}/Z_w, \tag{49}$$

where

$$Z_{s\nu}=\frac{\lambda_{\rm H}^2}{2\pi\hbar^2}\int_0^\infty w_{s\nu}(K_\perp)e^{\beta\chi_{s\nu}(K_\perp)}K_\perp dK_\perp, \tag{50}$$

$$Z_w=\sum_{s\nu}Z_{s\nu}. \tag{51}$$

The number of atoms per unit phase-space cell equals $[dN(\mathbf{K})/d^3K](2\pi\hbar)^3/V$. Calculation of $(U-TS)$ for this distribution gives

$$\begin{aligned}F_{\rm id}^{\rm H}&=k_BT\sum_{s\nu}N_{s\nu}\int\{\ln[n_{s\nu}\lambda_{\rm H}(2\pi\hbar)^2p_{s\nu}(K_\perp)]\\&\quad-1-\beta\chi_{s\nu}(K_\perp)\}p_{s\nu}(K_\perp)d^2K_\perp\\&=k_BT\sum_{s\nu}N_{s\nu}\int\ln\left[n_{s\nu}\lambda_{\rm H}^3\frac{w_{s\nu}(K_\perp)}{\exp(1)Z_{s\nu}}\right]p_{s\nu}(K_\perp)d^2K_\perp.\end{aligned} \tag{52}$$

The contribution of molecules should be added to this expression. We estimate it taking into account only the molecules in their ground state. This is an acceptable approximation at $B\gtrsim10^{12}$ G, because the energies of different types of molecular excitations are not much smaller than the electronic excitations of the atoms [61] (contrary to the zero-field case), so that excited levels cannot give a large contribution to the molecular IPF at those relatively low temperatures where the molecular fraction is large [20]. We also neglect the (unknown) motional modification of the molecular spectrum, as noted in Sec. IV A 2.

Thus, we include in the ideal free energy of the bound species $F_{\rm id}^{\rm neu}$ the term

$$F_{\rm id}^{\rm H_2}=N_{\rm H_2}k_BT[\ln(n_{\rm H_2}\lambda_{\rm H_2}^3)-1-\chi_{\rm H_2}], \tag{53}$$

where $\chi_{\rm H_2}=2\chi_{00}(0)+Q_2$ is the molecular binding energy, and Q_2 is the dissociation energy fitted as function of γ in [20,61].

The nonideal part $F_{\rm ex}^{\rm neu}$ is calculated in the hard-sphere approximation using Eqs. (17)–(19), where the composite atomic number is $\kappa=(s\nu K_\perp)$ and the obvious generalization of Σ_κ includes $\int p_{s\nu}(K_\perp)d^2K_\perp$. The effective atomic size $l_\kappa=l_{s\nu}(K_\perp)$ is given by fitting formulas [24]. The effective size of the H_2 molecule in the ground state is estimated as $l_{\rm H_2}=[2a_m^2+l_{z,{\rm H_2}}^2]^{1/2}$, where the longitudinal size is $l_{z,{\rm H_2}}\approx l_{z0}+r_0$. Here, l_{z0} is the longitudinal size of the ground-state H atom fitted in [24], and $r_0\approx12.7(\ln\gamma)^{-2.2}$ is the equilibrium internuclear separation given in [20].

C. Equilibrium conditions

The thermodynamic equilibrium for the free-energy model (46) is given by a generalization of the equations in Sec. II C, taking into account the fact that the atomic IPF Z_w now includes integration over $K_\perp$. In particular, $\partial F_{\rm ex}/\partial N_\kappa$ in Eq. (23) is replaced by a functional derivative.

In the conditions studied here, neutral atoms can exist only in the regime of strong magnetic quantization and weak degeneracy. Therefore it is convenient to write the generalized Saha equation using Eq. (34) and describe the deviations from it by a separate factor Λ. For the ideal free energy of protons, we use Eq. (35), and the one for the atoms is given by Eq. (52). Thus the generalized Saha equation reads

$$n_{\rm H}=n_p n_e \frac{\lambda_p \lambda_e (2\pi a_m^2)^2}{\lambda_{\rm H}^3}[1-\exp(-\beta\hbar\omega_{cp})] Z_w e^{\Lambda}, \tag{54}$$

where

$$\Lambda=\beta\mu_e-\ln(2\pi a_m^2\lambda_e n_e)+\beta\frac{\partial\mu_e}{\partial\ln n_e}-\frac{\partial P_e}{\partial n_e} \tag{55}$$

allows for deviations of the exact value of $F_{\rm id}^{(e)}$ from that given by Eq. (34) due to electron degeneracy and population of excited Landau levels. The distributions of atoms over the discrete quantum numbers and over the transverse pseudomomenta are given by Eqs. (49) and (48), respectively.

The occupation probabilities can be presented as a product of two terms that arise from $F_{\rm ex}^C$ and $F_{\rm HS}$:

$$w_{s\nu}(K_\perp)=w^C w_{s\nu}^{\rm HS}(K_\perp). \tag{56}$$

Hereafter, we exclude N_e from our formulas by explicit use of the electroneutrality condition $N_e=N_p$. Then the Coulomb factor reads

$$\ln w^C=\beta\frac{\partial F_{\rm ex}^C}{\partial N_p}=2f_{\rm ex}^C+\frac{2}{3}\left(\frac{\partial f_{\rm ex}^C}{\partial\ln\Gamma}-\frac{\partial f_{\rm ex}^C}{\partial\ln r_s}\right), \tag{57}$$

where $f_{\rm ex}^C(r_s,\Lambda)\equiv\beta F_{\rm ex}^C/(2N_p)$ is described in Sec. III B. In the Debye-Hückel limit, w^C is given by [32]

$$\ln w_{\rm DH}^C=-\sqrt{8\pi n_p(\beta e^2)^3}. \tag{58}$$

The hard-sphere factor reads

$$\ln w_{s\nu}^{\rm HS}(K_\perp)=\frac{(1-\eta/2)\ln w_{s\nu}^{(0)}(K_\perp)-5\eta^2+3\eta^3}{(1-\eta)^3}, \tag{59}$$

where $\ln w^{(0)}=(\partial/\partial N_p-\partial/\partial N_\kappa)[4N_{\rm tot}\eta]$ is the low-density limit of $\ln w^{\rm HS}$ and η is the packing fraction (18). Explicitly,

$$\ln w_{s\nu}^{(0)}(K_\perp)=-\frac{4\pi}{3}\{(n_{\rm H}+n_p)l_{s\nu}^3(K_\perp)+n_{{\rm H}_2}[l_{s\nu}(K_\perp)+l_{{\rm H}_2}]^3 +3n_{\rm H}[l_{s\nu}(K_\perp)\langle l^2\rangle+l_{s\nu}^2(K_\perp)\langle l\rangle]\}, \tag{60}$$

$$\eta=\frac{\pi}{3N_{\rm tot}V}[N_{\rm H}^2(\langle l^3\rangle+3\langle l^2\rangle\langle l\rangle)+N_{\rm H}N_p\langle l^3\rangle+N_{\rm H}N_{{\rm H}_2}(\langle l^3\rangle +3\langle l^2\rangle l_{{\rm H}_2}+3\langle l\rangle l_{{\rm H}_2}^2+l_{{\rm H}_2}^3)+N_p N_{{\rm H}_2}l_{{\rm H}_2}^3+4N_{{\rm H}_2}^2 l_{{\rm H}_2}^3], \tag{61}$$

where

$$\langle l^k\rangle\equiv\frac{1}{N_{\rm H}}\sum_{s\nu}N_{s\nu}\int l_{s\nu}^k(K_\perp)p(K_\perp)d^2K_\perp. \tag{62}$$

The dissociation equilibrium is given by Eq. (25), where Z_{w2} is replaced by $w_{{\rm H}_2}\exp(\chi_{{\rm H}_2})$ and Z_w is modified according to Eqs. (50) and (51). From Eq. (26) we obtain $w_{{\rm H}_2}=(w^C)^2 w_{{\rm H}_2}^{\rm HS}$, where

$$\ln w_{{\rm H}_2}^{\rm HS}=\frac{(1-\eta/2)\ln w_{{\rm H}_2}^{(0)}-15\eta^2+9\eta^3}{(1-\eta)^3}, \tag{63}$$

$$\ln w_{{\rm H}_2}^{(0)}=-\frac{4\pi}{3}[n_{\rm H}(3\langle l^2\rangle l_{{\rm H}_2} +3\langle l\rangle l_{{\rm H}_2}^2-\langle l^3\rangle)+(n_{\rm H}+n_p+6n_{{\rm H}_2})l_{{\rm H}_2}^3]. \tag{64}$$

A solution of Eqs. (54)–(64), supplemented by the stoichiometric constraint $n_p+n_{\rm H}+2n_{{\rm H}_2}=n_0$, yields the equilibrium abundances and the free-energy value. The solution is sought by an iteration procedure, in analogy with the zero-field case described in Sec. II C, and the EOS is obtained from Eq. (27). In the strongly quantizing magnetic field and in the nondegenerate regime, the EOS is a sum of three analytic terms: the ideal term $P_{\rm id}=n_{\rm tot}k_BT+(4\sigma/3c)T^4$, the contribution due to the Coulomb nonideality given by derivation of the fit described in Sec. II B, and the hard-sphere contribution $P_{\rm HS}=4\eta(1-\eta/2)(1-\eta)^{-3}n_{\rm tot}k_BT$.

V. RESULTS

A. Distribution of plasma particles

1. Occupation numbers

Figure 5 displays the distribution of the atoms over quantum states given by Eq. (49) at $B=10^{12}$ G and 10^{13} G, $T=10^6$ K, and at two relatively low densities $\rho=0.001\,{\rm g\,cm^{-3}}$ and 0.1 g cm^{-3}. The left panel shows the relative occupation numbers for the tightly bound states $\nu=0$, for different quantum numbers s. The distribution is broader for higher density. This apparently surprising feature is easily explained by the presence of the third quantum parameter $K_\perp$, in addition to s and ν. At low density most atoms reside in the states with large values of $K_\perp$ because of the large statistical weight of such states, which all have $s=0$ (Sec. IV A 1). At higher density, these strongly decentered states are removed by excluded-volume effects, and the distribution over s grows broader. Conversely, on the neighboring panel we observe a narrower distribution over ν

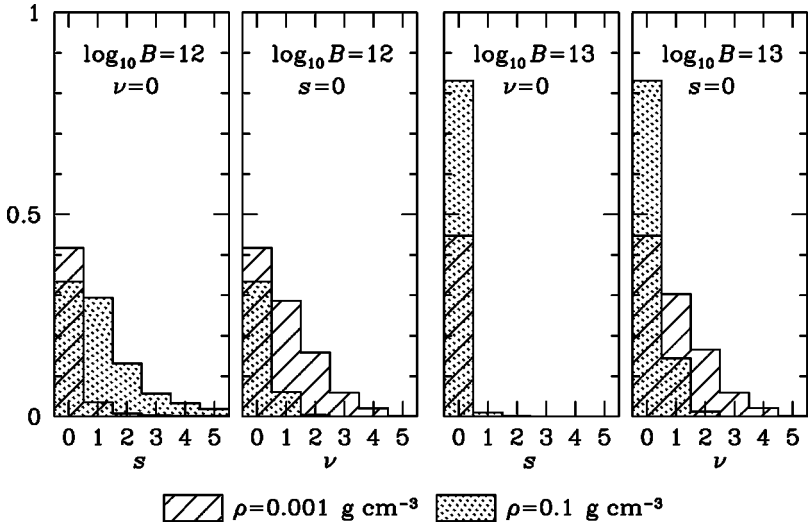

FIG. 5. Distribution of atomic occupation numbers at $T=10^6$ K for the magnetic field strengths $B=10^{12}$ G and 10^{13} G (indicated). For each value of B, the distribution over the quantum number s at $\nu=0$ and over ν at $s=0$ is shown for two density values: $\rho=0.001\ \mathrm{g\,cm^{-3}}$ (hatched histograms) and $0.1\ \mathrm{g\,cm^{-3}}$ (shaded histograms).

at higher density, because the excluded-volume effects eliminate the hydrogenlike states. In the next section we shall see that ultimately, at still larger densities, only the ground-centered state survives ($s=\nu=0$, $K_\perp<K_c$).

The right two panels demonstrate the effect of increasing B to 10^{13} G. Due to the larger binding energies, the distribution at $\rho=0.1\ \mathrm{g\,cm^{-3}}$ has become narrow, with more atoms concentrated in the ground state. However, at the lower density, the distribution over ν has changed weakly, since the increase of binding energies is accompanied by a decrease of the atomic size (and hence a decrease of the nonideality effects).

2. Ionization equilibrium

Figure 6 shows the ionization curves at three values of T for $B=10^{12}$ G. The heavy solid lines represent the total fraction of atoms $f_{\mathrm{H}}=n_{\mathrm{H}}/n_0$ in all quantum states, calculated according to Eq. (54). Thin solid lines show the fraction f_{00} of atoms in the ground state ($s=\nu=0$, but any $K_\perp$), and the dashed lines show the fraction of atoms in the centered states ($K_\perp<K_c$, any s and ν). For reference, triangles display the zero-field atomic fraction given by Eq. (20).

We see that a strong magnetic field generally increases the neutral fraction. At low densities, the excited atoms contribute significantly. Since their effective size is proportional to $K_\perp$, the integration (50) gives roughly $Z_{s\nu}\propto n_0^{-2/3}$; therefore f_{00} decreases asymptotically as $n_0^{1/3}$. Because of the broadening of the ν distribution (roughly, $\max\nu\propto n_0^{-1/6}$), the low-density wing of the curve for the total neutral fraction has a slope $f_{\mathrm{H}}\propto n_0^{1/6}$, which is very moderate compared to $f_{\mathrm{H}}\propto n_0^{1/2}$ in the nonmagnetic case (triangles).

The centered atoms, whose pseudomomentum is limited from above by the critical value K_c, have a nearly density-independent IPF at low ρ. Therefore their fraction behaves as $f_{\mathrm{cen}}\propto n_0$, and they disappear much faster at low ρ and especially at high T (compare the dashed lines in the upper and lower panels).

At high densities, on the contrary, the decentered states become depleted due to the excluded-volume effects, so that the dashed line in the figure merges with the solid one at $\rho\gtrsim 10\ \mathrm{g\,cm^{-3}}$. At still higher densities $\rho\gtrsim 10^2\ \mathrm{g\,cm^{-3}}$, all excited states disappear, and only the state $s=\nu=0$ survives. The pressure ionization proceeds around $\rho\sim 10^2-10^3\ \mathrm{g\,cm^{-3}}$. The excluded-volume and Coulomb nonideal effects favor pressure ionization [both w^{HS} and w^C in Eq. (56) are less than unity], whereas finite electron degeneracy hampers it ($\Lambda>0$). Because of the reduced atomic volume, the pressure ionization occurs at densities orders of magnitude larger than for the zero-field case [34]. At $T=10^{5.5}$ K, the molecular fraction becomes non-negligible at $\rho\sim 10^2\ \mathrm{g\,cm^{-3}}$.

Not all of the neutral atoms that contribute to the EOS may be identified spectroscopically. Because of their perturbation by plasma microfields, the atoms that do not satisfy the Inglis-Teller criterion form ''optical continuum.'' An approximate estimate of the fraction of atoms below the optical continuum is given by a generalization of the optical occupation probabilities $\tilde{w}_\kappa$ (Sec. II D) to the case of the strong magnetic field according to Eq. (14) of Ref. [65]. This ''IT'' fraction is shown by the long-dashed lines. Their rapid decrease indicates that the atomic spectral features disappear around $\rho\sim 10\ \mathrm{g\,cm^{-3}}$, long before pressure ionization.

The approximation of Lai and Salpeter [20], also shown in the figure (dotted line), clearly underestimates the neutral fraction at low density and overestimates it at high density, especially at high temperature. At low density, the discrepancy arises mainly from an underestimation of the decentered states because of an incorrect fitting formula to their binding energies. From a comparison with the dashed line in Fig. 6, we see that the fraction of centered states can be estimated by the approximation [20] at $\rho<0.1\ \mathrm{g\,cm^{-3}}$ and $T<10^6$ K. At higher T or larger ρ, the atomic abundance is overestimated in [19,20] because of neglecting nonideal effects. Although the neutral fraction is very significant, it never dominates the plasma at the values of T and B shown in Fig. 6, contrary to the prediction of Ref. [20]. (At $T=10^{5.5}$ K, the maximum is $f_{\mathrm{H}}=0.41$ at $\rho\approx 5\ \mathrm{g\,cm^{-3}}$.)

Figure 7 shows the ionization curves for a stronger field, $B=10^{13}$ G. Under this condition, the neutral fraction still increases. At $T=10^{5.5}$ K (top panel), f_{H} exceeds $\frac{1}{2}$ at $\rho>0.1\ \mathrm{g\,cm^{-3}}$, reaching the maximum of 85% at $\rho\approx 10$. Most atoms in this regime reside in the centered ground state. On the other hand, at $T=10^{5.5}$ K and $\rho\sim 10^2-10^3\ \mathrm{g\,cm^{-3}}$, the molecules are the dominant species; hence our present model

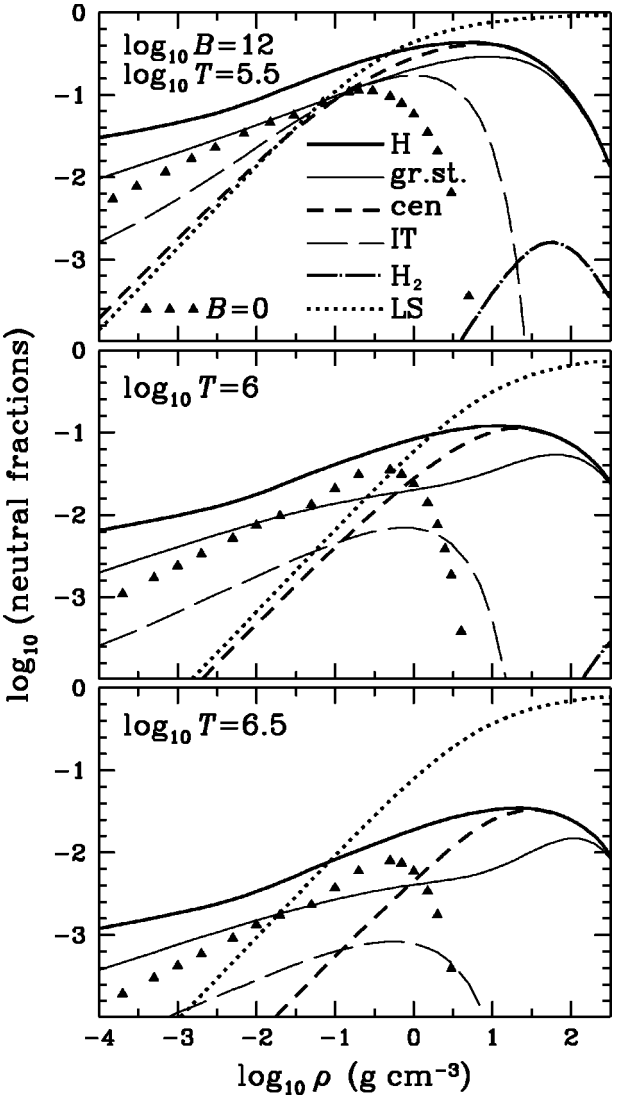

FIG. 6. Ionization isotherms at $B=10^{12}$ G and three values of T (indicated): total fraction of atoms $f_{\rm H}=n_{\rm H}/n_0$ (heavy solid lines) and the fractions of ground-state atoms (thin solid lines), the centered atoms (short-dashed lines), and the optically identifiable (Inglis-Teller) atoms (long-dashed lines). The dot-dashed lines show the molecular fraction $f_{\rm H_2}=2n_{\rm H_2}/n_0$, which is below the frame in the bottom panels. For comparison, $f_{\rm H}$ in the zero-field case (triangles) and in the approximation of Lai and Salpeter (dotted lines) is also shown.

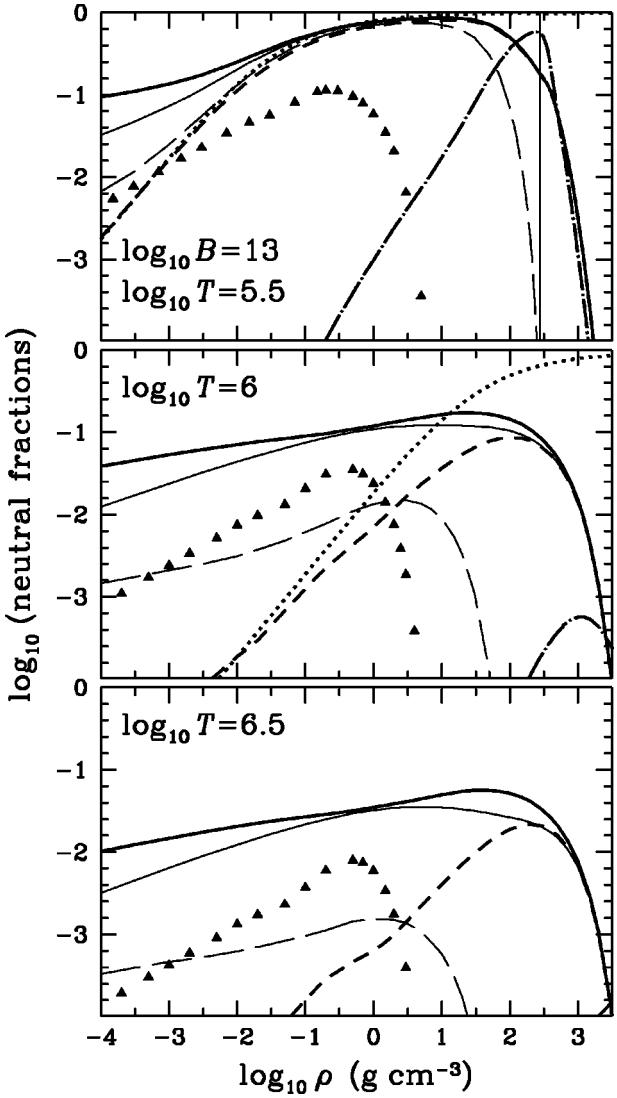

FIG. 7. The same as in Fig. 6 for $B=10^{13}$ G. The vertical line in the top panel separates the region of thermodynamic instability.

may be not accurate in this ρ-T domain.

A comparison with the result by Lai and Salpeter is not performed for $T=10^{6.5}$ K (the bottom panel of Fig. 7) because the approximations (3.11), (3.12) of Ref. [20] yield a negative IPF in this case.

At $T=10^{5.5}$ K and $\rho\gtrsim 300\,{\rm g\,cm^{-3}}$, there appears thermodynamic instability ($\partial P/\partial\rho<0$) leading to a phase transition. The stability is recovered at $\rho\gtrsim 8000\,{\rm g\,cm^{-3}}$, where the plasma is fully ionized. This phase transition is a complete analogue to the plasma phase transition (PPT) predicted in the zero-field case by several theoretical models [34,66] but not yet confirmed in experiment. It is caused by a strong Coulomb attraction between pressure-ionized plasma particles, which contributes negative pressure that cannot be compensated at low temperature until the degeneracy sets in. There is no confidence in the reality of the PPT because of its model dependence. In our case, an additional uncertainty is introduced by the simplified treatment of molecules.

The B dependence of the atomic fraction at two values of T and two values of ρ is shown in Fig. 8. The total $f_{\rm H}$ is drawn by solid lines and the ''optical'' (Inglis-Teller) fraction by dashed lines. Triangles in the left panel show the total fraction of atoms at $B=0$ (it is negligible at $\rho=10\,{\rm g\,cm^{-3}}$ on the right panel). Dotted lines correspond to the approximation [20] at $T=10^{5.5}$ K.

It was found previously [10,11] that the ionization degree decreases with growing B above $\sim 10^{12}$ G only at $T\lesssim 5\times 10^5$ K but, in contrast to the present results, increases at higher T. This behavior was attributed to two effects: decreasing phase space occupied by a plasma particle with growing B, which favors ionization, and increasing binding energy, which disfavors it. Our present result arises from the motional perturbations of the atoms, neglected in [10,11]: first, increasing B increases the effective mass $m^{\perp}$ and thus the statistical weight of the centered atoms, and second, at low densities the atomic IPF is further increased due to the decentered states.

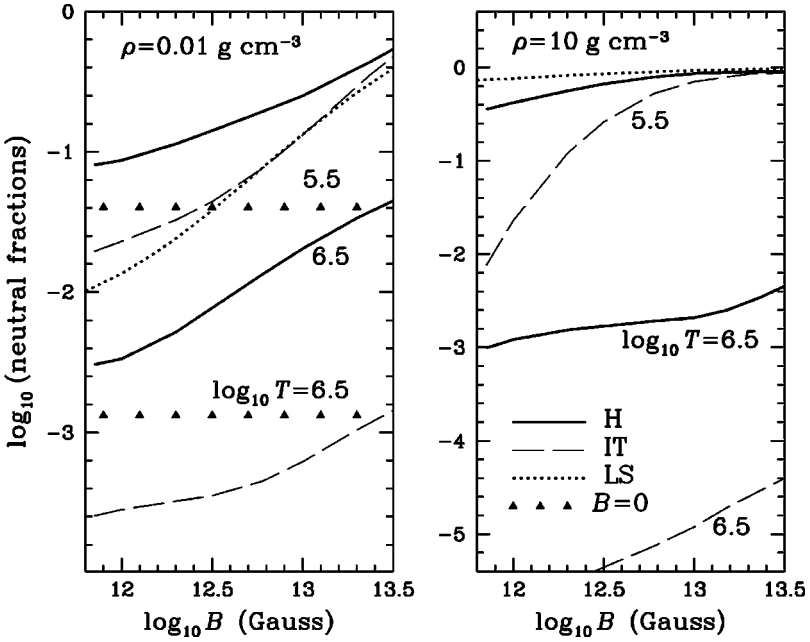

FIG. 8. Dependence of the atomic fraction f_H (solid lines) and the fraction of the optically identifiable atoms (dashed lines) on the magnetic field strength at two values of ρ (indicated in the figure), $T=10^{5.5}$ K (upper curves) and $10^{6.5}$ K (lower ones). The atomic fraction at $B=0$ (triangles) and the approximation of Ref. [20] (dotted lines) are shown for comparison.

B. Equation of state

Figure 9 presents four pressure isotherms obtained using the free-energy model described in Sec. IV. For comparison, we also show the fully ionized ideal-gas EOS (Sec. III A) and the nonmagnetic EOS (Sec. II). The vertical line bounds the region $\rho<\rho_B$. Let us first discuss the low-density regime $\rho\lesssim 10\,\mathrm{g\,cm^{-3}}$. At $T\gtrsim 10^6$ K, all three EOS reduce to $P=n_0k_BT$. At lower temperatures, the pressure deviates from this law because of the partial recombination of atoms. As discussed in the previous section, a strong magnetic field increases the neutral fraction; therefore the pressure is reduced more significantly compared to the $B=0$ case.

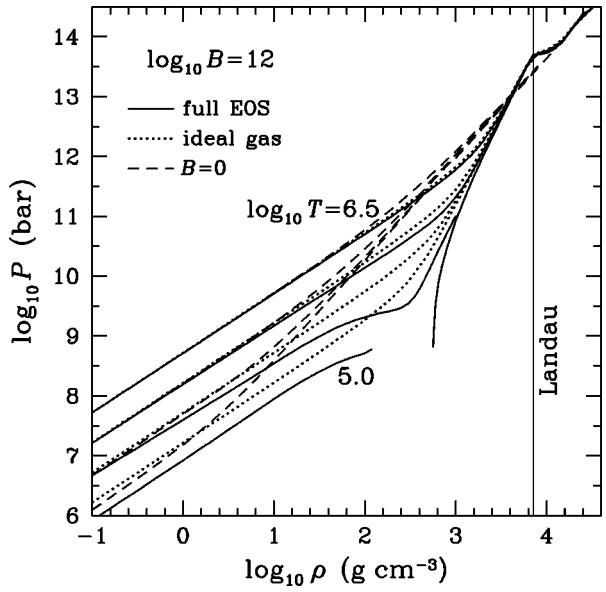

FIG. 9. EOS of partially ionized atomic hydrogen at $B=10^{12}$ G (solid lines) compared with the EOS of fully ionized ideal electron-proton plasma (dotted lines) and the EOS of partially ionized hydrogen at $B=0$ (dashed lines). The temperature logarithms are (from top to bottom) $\log T[K]=6.5$, 6.0, 5.5, and 5.0. The vertical line corresponds to ρ_B, above which excited Landau levels become populated.

In the intermediate-density range $10\,\mathrm{g\,cm^{-3}}\lesssim\rho\lesssim\rho_B$, the differences among the three considered cases are most important. For $B=0$, the plasma is fully ionized in this region, and the electrons become partially degenerate, making the EOS stiffer. In a strong magnetic field, the electron degeneracy is reduced (Sec. III); hence the ideal-gas EOS is softer, except for densities approaching ρ_B, where the degeneracy sets in and pressure grows rapidly. Partial recombination and Coulomb nonideality lead to a still further decrease of P. The pressure ionization discussed above has two opposite effects on the pressure: the positive ideal-gas contribution of free electrons appearing in the course of the ionization and the positive nonideal pressure of neutral species compete with the negative Coulomb contribution. At low T, these effects may cause the thermodynamic instability mentioned above, which we observe on the isotherm $T=10^5$ K. The second lowest isotherm in the figure is slightly overcritical for this PPT. The dependence of the critical temperature T_c and density ρ_c on B can be fitted by simple power laws $T_c=3\times10^5B_{12}^{0.39}$ K and $\rho_c=143B_{12}^{1.18}\,\mathrm{g\,cm^{-3}}$, where $B_{12}\equiv B/(10^{12}\,\mathrm{G})$. These fits provide an accuracy of a few percent in the considered range of the field strengths $7\times10^{11}\,\mathrm{G}<B<3\times10^{13}\,\mathrm{G}$.

At higher density $\rho\gtrsim\rho_B$, excited Landau levels become populated due to the increase of the Fermi energy. Eventually, at $\rho\gg\rho_B$, the nonmagnetic EOS is recovered.

Figure 10 demonstrates the effects of the strong magnetic field on the density exponent $\chi_\rho=(\partial\ln P/\partial\ln\rho)_T$. Although the pressure approaches the nonmagnetic value at $\rho>\rho_B$, the effects of magnetic quantization remain quite prominent for the derivative χ_ρ, as shown by the curve $B=10^{12}$ G in the figure. Consecutive population of excited Landau levels causes the oscillations of χ_ρ and other second derivatives of F around their nonmagnetic values. The regime where these oscillations are significant is called *weakly quantizing* [2].

The effects of a strongly quantizing magnetic field on the reduced heat capacity $C_V=k_B^{-1}(\partial U/\partial T)_V$ divided by the number of plasma particles, $N_{\mathrm{tot}}=N_e+N_p+N_{\mathrm{H}}+N_{\mathrm{H}_2}$, are shown in Fig. 11. In the nonmagnetic case (dashed line), the

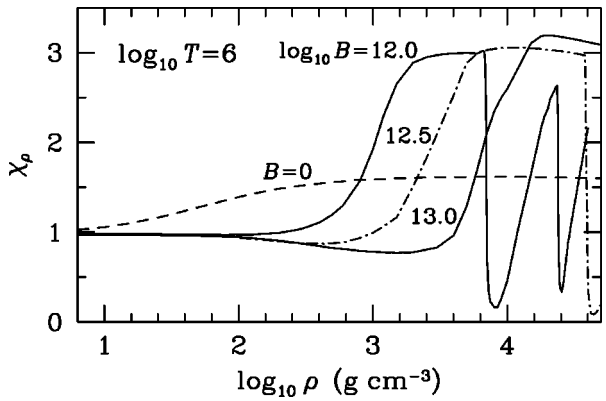

FIG. 10. Density exponent $\chi_\rho=(\partial \ln P/\partial \ln \rho)_T$ at $T=10^6$ K without magnetic field (dashed line) and in strong magnetic fields of various indicated strengths (dot-dashed and solid lines).

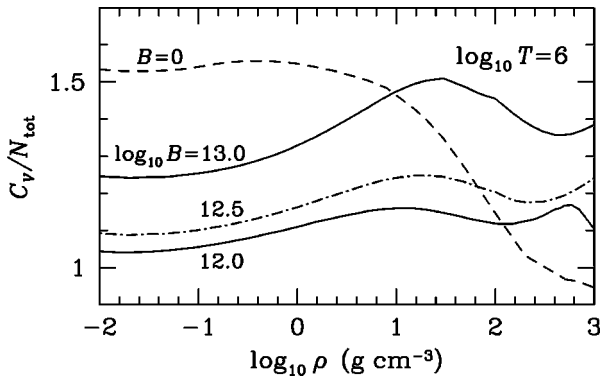

FIG. 11. Normalized heat capacity at the same T and B values as in Fig. 10.

classical value $C_V/N_{\rm tot}=\frac{3}{2}$ is slightly exceeded at lower densities because of the thermal ionization of the atoms, and it is reduced to smaller values at higher densities because of electron degeneracy.

In strong magnetic fields, the heat capacity is modified due to several effects. In the low-density regime, C_V is reduced compared to the nonmagnetic value because of the quantization of the transverse motion of electrons and protons. The strongly quantized electrons have only one motional degree of freedom, so that their contribution reduces to $C_{V_e}=\frac{1}{2}N_e$. When protons are nonquantized and the plasma is fully ionized, this amounts to $C_V/N_{\rm tot}=1$. In the general case, the contribution of free spinless protons would be

$$C_{Vp}^{(1)}=\left[\frac{1}{2}+\left(\frac{\beta\hbar\omega_{cp}}{2\sinh\left(\beta\hbar\omega_{cp}/2\right)}\right)^2\right]N_p, \qquad (65)$$

which tends to $\frac{1}{2}$ at $\beta\hbar\omega_{cp}=0.732B_{12}/T_6\gg 1$, where the protons are strongly quantized. The interaction of a magnetic field with proton spin, according to Eq. (36), yields

$$C_{Vp}^{(2)}=\left[\frac{\beta g_p\hbar\omega_{cp}}{4\cosh\left(\beta g_p\hbar\omega_{cp}/4\right)}\right]^2 N_0, \qquad (66)$$

which vanishes in the limiting cases of $\hbar\omega_{cp}\ll k_BT$ and $\hbar\omega_{cp}\gg k_BT$. In the latter case, $C_V/N_{\rm tot}$ would tend to $\frac{1}{2}$ for the fully ionized plasma. In Fig. 11, however, this does not happen because of the contribution of neutral atoms, which are subject to thermal ionization in this ρ-T-B domain. On the contrary, C_V increases with increasing B, since the neutral fraction becomes larger. The two humps visible on each magnetic isotherm correspond to the regions of the pressure destruction of the first excited atomic state $s=1$, $\nu=0$ and the ground state $s=\nu=0$, respectively. In the latter case, C_V even exceeds the nonmagnetic value, because of the delayed onset of degeneracy. Only with density approaching ρ_B is the zero-field value of the heat capacity recovered.

This illustrates the main effects of a strongly quantizing magnetic field on a partially ionized hydrogen plasma. Other thermodynamic quantities, obtained within the framework of the present model, experience similar profound modifications.

VI. CONCLUSIONS

We have developed a thermodynamic model of hydrogen plasma in strong magnetic fields, making use of the available quantum-mechanical results for the fully ionized plasma and for the hydrogen bound species. Applicability of the developed model is limited to the temperatures T, densities ρ, and magnetic field strengths B at which formation of molecules and other bound species more complex than the H atoms may be neglected. This condition holds, for instance, at $B_{12}\lesssim 10$ and $T\gtrsim 10^6$ K (any ρ) or at $T\gtrsim 10^5$ K and $\rho\lesssim 10^4(T_6/B_{12})^3$ g cm^{-3}. Furthermore, although the theory presented in Sec. IV is rather general, our numerical results in partially ionized regions are restricted to $B_{12}\geqslant 0.7$, because fitting formulas [24] for quantum-mechanical characteristics of the atoms moving in magnetic fields have been derived under this condition. This restriction is fulfilled for the majority of neutron stars. For laboratory field strengths (at $\gamma\ll 1$), perturbative methods may be sufficient.

Calculations in the frames of our model show that the magnetic field effects strongly modify the thermodynamic functions and phase diagram of the plasma, in particular the partial ionization region. The abundance of atoms is significant in the considered domain of temperatures $T\sim 10^5$–$10^{6.5}$ K and magnetic field strengths $B\sim 10^{12}$–10^{13} G at densities up to $\rho\sim 10^2$–10^3 g cm^{-3}, contrary to the zero-field case. At relatively low densities ($\rho\lesssim 1$–100 g cm^{-3}, depending on B and T), the decentered atomic states possessing a large constant dipole moment are significantly populated. Since these values of ρ, T, and B are typical of the atmospheres of isolated neutron stars, the physical effects discussed above are expected to affect the spectra. It has been shown [65,67] that the presence of a nonionized component and, in particular, decentered atoms should produce observable absorption and thus necessitate a modification of previous fully ionized atmosphere models [68]. Work in this direction is under way [69].

ACKNOWLEDGMENTS

A.Y.P. is grateful to the theoretical astrophysics group at the Ecole Normale Supérieure de Lyon for hospitality and financial support. A.Y.P. and Y.A.S. acknowledge useful discussions with J. Ventura and (at the initial stage of the work) with G. G. Pavlov and V. E. Zavlin. We thank M. Steinberg for sending us some of his results prior to publication. The work of A.Y.P. and Y.A.S. has been partially supported by INTAS Grant No. 96-542 and RFBR Grant No. 99-02-18099.

[1] V. Canuto and J. Ventura, Fundam. Cosm. Phys. **2**, 203 (1977).

[2] D. G. Yakovlev and A. D. Kaminker, in *The Equation of State in Astrophysics*, edited by G. Chabrier and E. Schatzman (Cambridge University Press, Cambridge, England, 1994), p. 214.

[3] G. G. Pavlov, Yu. A. Shibanov, V. E. Zavlin, and R. D. Meyer, in *The Lives of the Neutron Stars*, edited by M. A. Alpar, Ü. Kiziloğlu, and J. van Paradijs (Kluwer, Dordrecht, 1995), p. 71.

[4] G. Chabrier, A. Y. Potekhin, and D. G. Yakovlev, Astrophys. J. **477**, L99 (1997); A. Y. Potekhin, G. Chabrier, and D. G. Yakovlev, Astron. Astrophys. **323**, 415 (1997).

[5] D. Page, Yu. A. Shibanov, and V. E. Zavlin, in *Röntgenstrahlung from the Universe*, MPE Report No. 263, edited by H. U. Zimmermann, J. Trümper, and H. Yorke (MPE, Garching, 1996), p. 173; D. Page, Astrophys. J. **479**, L43 (1997).

[6] D. H. Constantinescu and P. Rehák, Nuovo Cimento B **32**, 177 (1976); D. H. Constantinescu and G. Moruzzi, Phys. Rev. D **18**, 1820 (1978).

[7] I. Fushiki, E. H. Gudmundsson, and C. J. Pethick, Astrophys. J. **342**, 958 (1989).

[8] A. M. Abrahams and S. L. Shapiro, Astrophys. J. **374**, 652 (1991).

[9] Ö. E. Rögnvaldsson, I. Fushiki, E. H. Gudmundsson, C. J. Pethick, and J. Yngvason, Astrophys. J. **416**, 276 (1993); A. Thorolfsson, Ö. E. Rögnvaldsson, J. Yngvason, and E. H. Gudmundsson, *ibid.* **502**, 847 (1998).

[10] Yu. N. Gnedin, G. G. Pavlov, and A. I. Tsygan, Zh. Eksp. Teor. Fiz. **66**, 421 (1974) [Sov. Phys. JETP **39**, 301 (1974)].

[11] V. K. Khersonskii, Astron. Zh. **64**, 433 (1987) [Sov. Astron. **31**, 225 (1987)].

[12] V. K. Khersonskii, Astron. Zh. **64**, 1233 (1987) [Sov. Astron. **31**, 646 (1988)].

[13] L. P. Gor'kov and I. E. Dzyaloshinskii, Zh. Eksp. Teor. Fiz. **53**, 717 (1967) [Sov. Phys. JETP **26**, 449 (1968)].

[14] L. A. Burkova, I. E. Dzyaloshinskii, G. P. Drukarev, and B. S. Monozon, Zh. Eksp. Teor. Fiz. **71**, 526 (1976) [Sov. Phys. JETP **44**, 276 (1976)].

[15] M. Vincke, M. Le Dourneuf, and D. Baye, J. Phys. B **25**, 2787 (1992).

[16] G. G. Pavlov and P. Mészáros, Astrophys. J. **416**, 752 (1993).

[17] A. Y. Potekhin, J. Phys. B **27**, 1073 (1994).

[18] J. Ventura, H. Herold, H. Ruder, and F. Geyer, Astron. Astrophys. **261**, 235 (1992).

[19] D. Lai and E. E. Salpeter, Phys. Rev. A **52**, 2611 (1995).

[20] D. Lai and E. E. Salpeter, Astrophys. J. **491**, 270 (1997).

[21] M. Steinberg, J. Ortner, and W. Ebeling, Phys. Rev. E **58**, 3806 (1998).

[22] W. Ebeling, W. D. Kraeft, and D. Kremp, *Theory of Bound States and Ionization Equilibrium of Plasmas and Solids* (Akademie, Berlin, 1977).

[23] W. Däppen, L. Anderson, and D. Mihalas, Astrophys. J. **319**, 195 (1987).

[24] A. Y. Potekhin, J. Phys. B **31**, 49 (1998).

[25] W. Däppen, Rev. Mex. Astron. Astrofis. **23**, 141 (1992).

[26] G. Chabrier, in *The Equation of State in Astrophysics*, edited by G. Chabrier and E. Schatzman (Cambridge University Press, Cambridge, England, 1994), p. 287.

[27] E. Fermi, Z. Phys. **26**, 54 (1924).

[28] D. G. Hummer and D. Mihalas, Astrophys. J. **331**, 794 (1988).

[29] D. Mihalas, W. Däppen, and D. G. Hummer, Astrophys. J. **331**, 815 (1988).

[30] W. Däppen, D. Mihalas, D. G. Hummer, and B. W. Mihalas, Astrophys. J. **332**, 261 (1988); D. Mihalas, D. G. Hummer, B. W. Mihalas, and W. Däppen, *ibid.* **350**, 300 (1990).

[31] D. Saumon, G. Chabrier, and H. M. Van Horn, Astrophys. J., Suppl. Ser. **99**, 713 (1995).

[32] A. Y. Potekhin, Phys. Plasmas **3**, 4156 (1996).

[33] D. Saumon and G. Chabrier, Phys. Rev. A **44**, 5122 (1991).

[34] D. Saumon and G. Chabrier, Phys. Rev. A **46**, 2084 (1992).

[35] F. J. Rogers, Astrophys. J. **310**, 723 (1986).

[36] L. D. Landau and E. M. Lifshitz, *Statistical Physics* (Pergamon, Oxford, 1986), Pt. I.

[37] H. M. Antia, Astrophys. J., Suppl. Ser. **84**, 101 (1993).

[38] M. Baus and J. P. Hansen, Phys. Rep. **59**, 1 (1980).

[39] S. Ichimaru, H. Iyetomi, and S. Tanaka, Phys. Rep. **149**, 91 (1987).

[40] G. Chabrier, J. Phys. (Paris) **51**, 1607 (1990).

[41] G. Chabrier and A. Y. Potekhin, Phys. Rev. E **58**, 4941 (1998).

[42] H. DeWitt, W. Slattery, and G. Chabrier, Physica B **228**, 158 (1996).

[43] J. Jung, M. S. Jhon, and F. H. Ree, J. Chem. Phys. **100**, 528 (1994); **102**, 1349 (1995).

[44] N. F. Carnahan and K. E. Starling, J. Chem. Phys. **51**, 635 (1969).

[45] Following [32], we estimate $l_n = a_0 n \sqrt{7n^2+5}/2$ for an atom with principal quantum number n. This yields $d_{00} = a_0\sqrt{3}$, which is 13% smaller than the SC [34] hard-core diameters.

[46] In the partially degenerate regime, convergence of this procedure may be poor. In that case we impose a stabilization restriction that w_κ does not vary appreciably from its value at the preceding iteration.

[47] F. J. Rogers and C. A. Iglesias, Astrophys. J., Suppl. Ser. **79**, 507 (1992); C. A. Iglesias and F. J. Rogers, Astrophys. J. **464**, 943 (1996). We are grateful to F. J. Rogers for providing us with the monochromatic opacity tables.

[48] V. E. Zavlin, G. G. Pavlov, and Yu. A. Shibanov, Astron. Astrophys. **315**, 141 (1996).

[49] F. J. Rogers, F. J. Swenson, and C. A. Iglesias, Astrophys. J. **456**, 902 (1996).

[50] L. D. Landau and E. M. Lifshitz, *Quantum Mechanics* (Pergamon, Oxford, 1976).
[51] A. Y. Potekhin and D. G. Yakovlev, Astron. Astrophys. **314**, 341 (1996).
[52] F. Cornu, Europhys. Lett. **37**, 591 (1997); Phys. Rev. E **58**, 5268 (1998); **58**, 5293 (1998).
[53] R. W. Danz and M. L. Glasser, Phys. Rev. B **4**, 94 (1971).
[54] F. Perrot and C. Dharma-wardana, Phys. Rev. A **30**, 2619 (1984).
[55] A. Alastuey and B. Jancovici, Physica A **102**, 327 (1980).
[56] H. E. DeWitt, M. Schlanges, A. Y. Sakakura, and W. D. Kraeft, Phys. Lett. A **197**, 326 (1995); see also A. Alastuey and A. Perez, Phys. Rev. E **53**, 5714 (1996).
[57] E. E. Salpeter, Astrophys. J. **134**, 669 (1961).
[58] It was recently suggested, however, that this same large separation in the decentered states may help to create a positronium atom stable against the annihilation in the laboratory [J. Ackermann, J. Shertzer, and P. Schmelcher, Phys. Rev. Lett. **78**, 199 (1997); J. Shertzer, J. Ackermann, and P. Schmelcher, Phys. Rev. A **58**, 1129 (1998)].
[59] U. Wille, J. Phys. B **20**, L417 (1986); Phys. Rev. A **38**, 3210 (1987); U. Kappes and P. Schmelcher, *ibid.* **53**, 3869 (1996).
[60] D. Neuhauser, S. E. Koonin, and K. Langanke, Phys. Rev. A **36**, 4163 (1987); D. Lai, E. E. Salpeter, and S. L. Shapiro, *ibid.* **45**, 4832 (1992).
[61] D. Lai and E. E. Salpeter, Phys. Rev. A **53**, 152 (1996).
[62] Yu. P. Kravchenko and M. A. Liberman, Phys. Rev. A **55**, 2701 (1997).
[63] T. Detmer, P. Schmelcher, F. K. Diakonos, and L. S. Cederbaum, Phys. Rev. A **56**, 1825 (1997), and references therein; T. Detmer, P. Schmelcher, and L. S. Cederbaum, *ibid.* **57**, 1767 (1998).
[64] M. A. Ruderman, Phys. Rev. Lett. **27**, 1306 (1971).
[65] G. G. Pavlov and A. Y. Potekhin, Astrophys. J. **450**, 883 (1995).
[66] G. E. Norman and A. N. Starostin, High Temp. **6**, 394 (1968); W. Ebeling and W. Richert, Phys. Lett. **108A**, 80 (1985); G. A. Baker, Phys. Rev. E **56**, 5216 (1997).
[67] A. Y. Potekhin and G. G. Pavlov, Astrophys. J. **483**, 414 (1997).
[68] Yu. A. Shibanov, G. G. Pavlov, V. E. Zavlin, and J. Ventura, Astron. Astrophys. **266**, 313 (1992).
[69] Preliminary results have been presented by A. Y. Potekhin, Yu. A. Shibanov, and J. Ventura, in *Neutron Stars and Pulsars*, edited by N. Shibazaki, N. Kawai, S. Shibata, and T. Kifune (Universal Academy Press, Tokyo, 1998), p. 161.